PCCP

ROYAL SOCIETY OF CHEMISTRY

PAPER

View Article Online
View Journal

Cite this: DOI: 10.1039/c8cp05597a

Infrared photodissociation spectroscopy of ion-radical networks in cationic dimethylamine complexes†

Xin Lei,‡[ab] Xiangtao Kong,‡[a] Zhi Zhao,[a] Bingbing Zhang,[ab] Dongxu Dai,[a] Xueming Yang[a] and Ling Jiang*[a]

Received 4th September 2018,
Accepted 22nd October 2018

DOI: 10.1039/c8cp05597a

rsc.li/pccp

Infrared photodissociation spectroscopy was employed to establish the general trends in the stepwise growth motif of cationic dimethylamine $(DMA)_n^+$ (n = 4–13) complexes. Electronic structure calculations were performed to identify the structure of the low-lying isomers and to assign the observed spectral features. The results showed the preference of the formation of the proton-transferred $(CH_3)_2NH_2^+$ ion core. The $(CH_3)_2NH_2^+$–$[(CH_3)_2N]$ ion-radical pair contact and the ion-radical separated pair could coexist at n = 4. The $[(CH_3)_2N]$ radical is separated from the $(CH_3)_2NH_2^+$ ion core by one DMA molecule at n = 4–6 and by two or more DMA molecules in the larger clusters. This suggests that the $(CH_3)_2NH_2^+$–$[(CH_3)_2N]$ ion-radical contact pair is not stable in the subsequent radiation-induced processes of DMA, and the $[(CH_3)_2N]$ radical is released from the charged site in the cationic DMA networks.

1. Introduction

The study of ionizing radiation is of significant interest because of its crucial role in various fields such as nuclear reactors, waste remediation and environmental cleanup, and medical diagnosis and therapy.[1] Radiation-induced chemical processes could create radicals and ions, which react with other species to form a variety of complexes.[2] Understanding of the properties and processes of energetic species in aqueous systems is complicated due to the presence of different local environments. Clusters play a vital role in understanding this radiation chemistry by allowing us to isolate particular hydrogen-bonded morphologies and then to predict how these networked "supermolecules" adapt and rearrange when exposed to ionizing radiation.[1] Mass spectrometry and optical spectroscopy of gas-phase clusters provide detailed energetic and structural information that is difficult to extract from bulk measurements.[3–9] The radiolysis of water has been extensively studied because of its important role in electron-initiated processes and radical chemistry.[1] The infrared photodissociation (IRPD) spectroscopic study of $H_4O_2^+{\cdot}Ar$ and $H_4O_2^+{\cdot}Ar_2$ complexes has identified the H_3O^+–OH ion-radical contact pair structure.[10] Spectroscopic and theoretical investigations of larger $(H_2O)_n^+$ clusters have demonstrated that the H_3O^+ ion core is preferentially solvated with water, and the OH radical is separated from the H_3O^+ ion core by at least one water molecule in the $n \geq 5$ clusters.[11–14]

Previous investigations of $(NH_3)_n^+$ (n = 2–4) have shown that the cluster cations have the proton-transferred type structures with the formation of a pair of a protonated cation and a neutral radical, NH_4^+–NH_2.[15] The gas-phase vibrational spectroscopic study of the cationic trimethylamine dimer, $(TMA)_2^+$, revealed the coexistence of the charge-shared N···N type and proton-transferred C···HN type structures.[16] Our recent infrared spectroscopic and computational results indicated that the charge-shared N···N type $(TMA)_2^+$ ion core is preferred in the cold cationic trimethylamine $(TMA)_n^+$ (n = 3–9) clusters.[17] The dimethylamine (DMA) complex is one of the molecules having one polar NH group and two nonpolar CH_3 groups, which affords a model system for studying the proton transfer in the ionizing radiation-induced processes of the species that contains both NH and CH_3 groups. On the other hand, DMA plays an important role in enhancing particle nucleation and affecting secondary organic aerosol formation.[18,19] A number of questions of the $(DMA)_n^+$ clusters are of fundamental interest for the molecular-level understanding of relevant chemical and atmospheric processes: (1) what factors are essential for the stepwise growth motif; (2) which one is the preference in-between the proton-transferred and charge-shared structures; (3) if the proton-transferred structure is formed, how many DMA molecules are needed to separate the $(CH_3)_2N$ radical from the

---

[a] State Key Laboratory of Molecular Reaction Dynamics, Collaborative Innovation Center of Chemistry for Energy and Materials (iChEM), Dalian Institute of Chemical Physics, Chinese Academy of Sciences, 457 Zhongshan Road, Dalian 116023, China. E-mail: ljiang@dicp.ac.cn

[b] University of Chinese Academy of Sciences, 19A Yuquan Road, Beijing 100049, China

† Electronic supplementary information (ESI) available. See DOI: 10.1039/c8cp05597a

‡ These authors contributed equally to this work.

$(CH_3)_2NH_2^+$ ion core, *etc.* Herein, we report the gas-phase infrared spectra of the $(DMA)_n^+$ (n = 4–13) clusters. The $(DMA)_n^+$ cations were generated by the ionization of pulsed supersonic beams *via* a dielectric barrier discharge (DBD) source[20] and characterized using mass-selected infrared multiple photon dissociation (IRMPD) spectroscopy. The structural assignment of the IRMPD spectra was aided by quantum chemical calculations. The combination of experimental and calculated IR spectra allows for the identification of the general trends in the stepwise growth motif of the $(DMA)_n^+$ complexes.

2. Experimental details

IRMPD experiments were carried out using an ion-trap mass spectrometer described previously.[17] A supersonic beam of DMA complexes was produced from the expansion using a dielectric barrier discharge (DBD) source. Cluster ions were passed through a 4 mm diameter skimmer. The ions of interest were selected using a quadrupole mass filter, deflected by 90° in an electrostatic quadrupole deflector, and focused into a radiofrequency 3D Paul trap guide. The mass resolution of the quadrupole mass filter was set to be sufficiently high ($\Delta m/z \leq \sim 1$) to prevent contamination by other cluster species. To allow for continuous ion accumulation and ion thermalization, the ion trap was continuously filled with helium buffer gas at an ion-trap temperature of 15 K. After loading the trap for 98 ms, all ions were extracted from the trap and focused both temporally and spatially into the center of the extraction region of an orthogonally mounted linear time-of-flight (TOF) mass spectrometer. Here, the ion packet was irradiated with a coaxial-propagating IR laser pulse. After IR laser irradiation, the fragment and parent ions were accelerated and mass analyzed using the TOF mass spectrometer. An IRMPD spectrum was recorded by monitoring all ion intensities simultaneously as a function of the dissociation IR laser wavelength. Typical spectra were obtained by scanning the dissociation laser in a step of 2 cm^{-1} and averaging over 600 laser shots at each wavelength. All the experimental spectra were normalized according to the IR power. The nearly linear laser power dependence of the fragmentation signal was confirmed.

A tunable infrared laser beam was generated using a KTP/KTA optical parametric oscillator/optical parametric amplifier system (OPO/OPA, LaserVision)[21] pumped by an injection-seeded Nd:YAG laser (Continuum Surelite EX). This table-top IR laser system provided tunable IR output radiation from 700 to 7000 cm^{-1} with a 7 ns pulse width. The linewidth of the mid-IR output was $\sim$1 cm^{-1}. Because of the limitation of the output power in the low-frequency region, reliable measurements were restricted above 2500 cm^{-1} in this experiment. The wavelength of the OPO laser output was calibrated using a laser spectrum analyzer (HighFinesse, OSA).

3. Theoretical methods

All calculations were carried out using the Gaussian 09 package.[22] Various methods have been tested for $(DMA)_n^+$ (n = 4–8). The MPW1K method yielded a better systematic agreement with the experimental results. Recent investigations have demonstrated that the MPW1K functional can well reproduce the infrared spectroscopic experiments of ion-radical networks in water clusters $(H_2O)_n^+$ (n = 3–11).[11] Therefore, this functional was employed for the present calculations as well. The 6-311+G(d,p) basis set was used for all the atoms. Tight convergence of the optimization and the self-consistent field procedures was imposed, and an ultrafine grid was used. MP2/6-311+G(d,p) single point calculations on the MPW1K/6-311 G(d,p) optimized structures were carried out to determine the relative energies and dissociation energies. Harmonic frequency calculations were performed. Calculated frequencies were scaled by a factor of 0.937.[23] The resulting stick spectra were convoluted by a Gaussian line shape function with a full width at half-maximum line width of 6 cm^{-1} in order to account for line-broadening effects. Considering that the G4(MP2) method could be an accurate and economical method for thermochemical predictions,[24] this method was used to explore the proton transfer of NH_3^+, $(CH_3)_2NH^+$, and $(CH_3)_3N^+$, and the dissociation channel of $(DMA)_4^+$. The G4(MP2) calculations were not carried out for $(DMA)_n^+$ ($n \geq 5$) because of the expensive computational cost. The details of G4(MP2) theory have been reported previously.[24]

4. Results and analysis

A typical quadrupole mass spectrum of cluster ions produced by the DBD source is shown in Fig. S1 (ESI†). The $(DMA)_n^+$ clusters are observed. Additional signals of the $C^+(DMA)_n$ and $(CNH_2)^+(DMA)_n$ species are also observed with relatively weak intensities as compared to $(DMA)_n^+$. The TOF mass spectrometer was used to confirm the mass distribution of the size-selected cluster. As shown in Fig. 1, the shoulder peaks labeled with "Δ" are due to the natural ^{13}C concentration, wherein intensities could be reproduced using the isotopic pattern simulation software.

The lowest dissociation energy of $(DMA)_3^+$ was calculated to be 85.81 kJ mol^{-1} at the MP2/6-311+G(d,p)//MPW1K/6-311+G(d,p) level of theory (Table S1, ESI†). Assuming that the internally cold $(DMA)_3^+$ is formed, the absorption of at least three photons around 3000 cm^{-1} is required to overcome the dissociation limit. The single pass of photon fluence generated using the table-top LaserVision system might be insufficient to induce the photofragmentation of $(DMA)_3^+$ under the present experimental conditions. Beginning at the n = 4 cluster, the fragmentation was observed. A higher fragmentation yield was obtained for the n = 5–13 clusters. The number densities of the $n \geq 14$ clusters are insufficient for the obvious detection of IR-induced-dissociation fragmentation. Fig. 2 shows the experimental IRMPD spectra of $(DMA)_n^+$ (n = 4–13) clusters. Only the loss of one or more DMA molecules was observed upon the IR vibrational excitation. The experimental IRMPD spectra comprise nine bands, labeled (A–I). Band positions are summarized in Table 1. Band A appears at 3165 cm^{-1} in the n = 5 cluster, which blue-shifts to 3180 cm^{-1} at n = 6 and is centered around

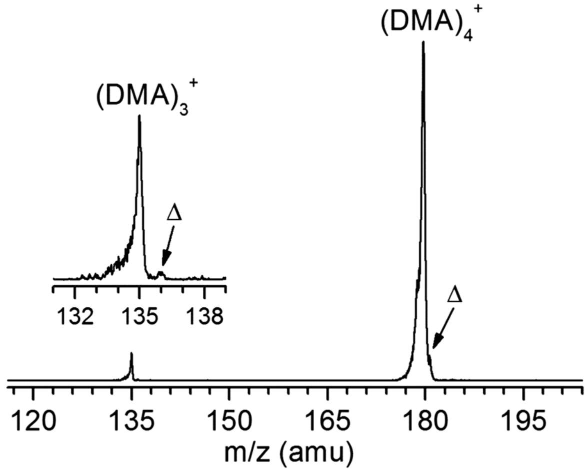

Fig. 1 TOF mass spectrum for the IR photodissociation of (DMA)$_4^+$ when IR laser is on. The mass spectrum in the 132–138 amu region is enlarged in the inset. The peaks labeled with "Δ" correspond to the contribution of the natural ^{13}C concentration.

3237 cm^{-1} in the larger clusters. Band B is centered at 3123 cm^{-1} in the n = 4 cluster, which blue-shifts slightly to 3133 cm^{-1} at n = 5 and is converged around 3150 cm^{-1} with increasing cluster size. Band C appears as a sharp peak at 2991 cm^{-1} at n = 4, which red-shifts slightly to 2976 cm^{-1} at n = 13. Similarly, bands D–I show small red-shifts by 9–30 cm^{-1}.

Present calculations for (DMA)$_n^+$ (n = 4–8) yielded the proton-transferred structures, in which the position of the [$(CH_3)_2N$] radical is different. For the weakly-bounded (DMA)$_n^+$ clusters, many local minima might exist. We will focus on three types of low-lying structures for simplicity, which include the ion-radical separated pair with chain or ring structures and the ion-radical contact pair with chain structures. Fig. 3 illustrates the optimized structures. The comparison of the experimental IRMPD spectrum to the calculated IR spectra is shown in Fig. 4–8, respectively, in which capital letters (A, B, C, . . .) are used for experimental peaks and lower case letters (a, b, c, . . .) for theoretical ones.

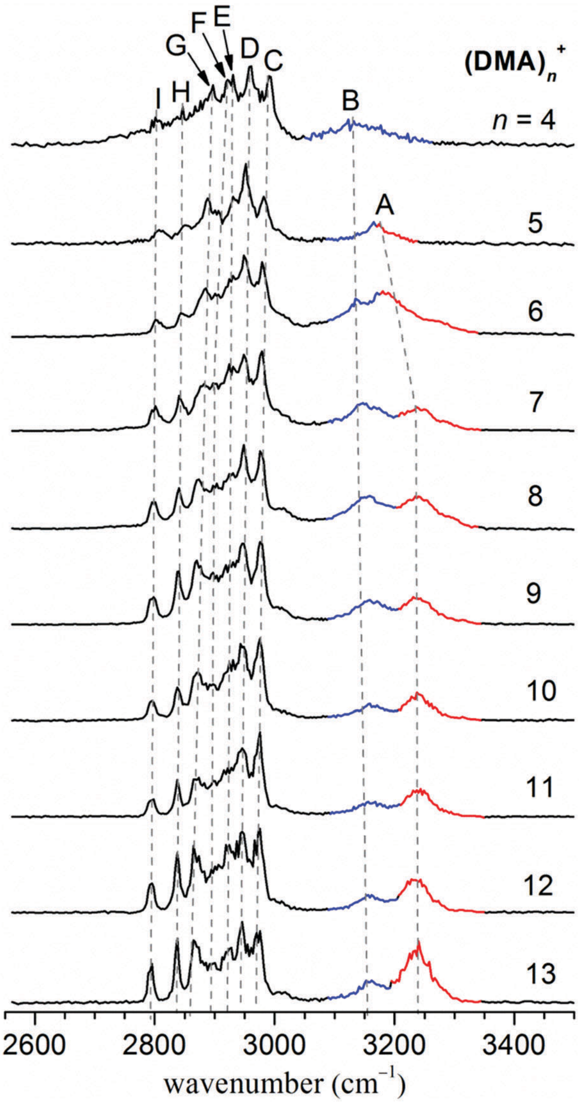

Fig. 2 Experimental IRMPD spectra of (DMA)$_n^+$ ions with n = 4–13.

(DMA)$_4^+$

The lowest-energy isomer (4-I) has a ring structure with the formation of the proton-transferred $(CH_3)_2NH_2^+$ ion core and the $(CH_3)_2N$ radical (Fig. 3). Isomer 4-II has a chain structure with an ion-radical separated pair, in which the $(CH_3)_2N$ radical is separated from the $(CH_3)_2NH_2^+$ ion core by one DMA molecule. 4-II lies only 2.40 kJ mol^{-1} higher than 4-I. Isomer 4-III (+5.52 kJ mol^{-1}) consists of an ion-radical contact pair. The lowest dissociation energies for reactions (1) and (2) are endothermic by 54.08 and 70.10 kJ mol^{-1} calculated at the G4(MP2) level, respectively.

$$[(CH_3)_2NH]_4^+ \rightarrow [(CH_3)_2NH]_3^+ + (CH_3)_2NH \quad (1)$$

$$[(CH_3)_2NH]_4^+ \rightarrow H^+[(CH_3)_2NH]_3 + (CH_3)_2N \quad (2)$$

This suggests that the loss of one DMA molecule from (DMA)$_4^+$ is more favorable than the loss of the [$(CH_3)_2N$] radical upon the IR vibrational excitation, supporting the observed fragment feature that only the loss of the DMA molecule occurs upon infrared photodissociation.

In the calculated IR spectrum of 4-I (Fig. 4), the 3303 cm^{-1} band (labeled b) is due to the H-bonded N–H stretch of the first coordinated (1-coord) DMA towards the $(CH_3)_2NH_2^+$ ion core, which is close to the upper edge of the experimental broad band B. The calculated band c at 2994 cm^{-1} is attributed to the CH_2 antisymmetric stretch of neutral DMA with the movement of only two H atoms inside methyl groups, which is consistent with the experimental value of band C (2991 cm^{-1}). The CH_3 antisymmetric stretch of neutral DMA is predicted at 2962 cm^{-1} (band d), which agrees with the experimental value of band D (2961 cm^{-1}). The CH_3 symmetric stretch of the $(CH_3)_2NH_2^+$ ion core is predicted at 2938 cm^{-1} (band e), which is observed experimentally at 2931 cm^{-1} (band E). The calculated band f at 2920 cm^{-1} is assigned to the CH_2 antisymmetric stretch of the [$(CH_3)_2N$] radical, which reproduces the

Table 1 Peak positions (in cm^{-1}) in the experimental IRMPD spectra of $(DMA)_n^+$ (n = 4–13)

Label	n = 4	n = 5	n = 6	n = 7	n = 8	n = 9	n = 10	n = 11	n = 12	n = 13	Assignment
A		3165	3180	3237	3240	3237	3237	3238	3239	3240	H-Bonded N–H stretch of 2-coord DMA
B	3180, 3123	3133	3135	3141	3147	3150	3152	3153	3156	3156	H-Bonded N–H stretch of 1-coord DMA
C	2991	2982	2979	2978	2977	2976	2976	2976	2976	2976	CH_2 antisymmetric stretch of neutral DMA
D	2961	2952	2949	2948	2948	2947	2946	2945	2945	2945	CH_3 antisymmetric stretch of neutral DMA
E	2931	2930	2928	2927	2924	2923	2923	2921	2920	2920	CH_3 symmetric stretch of the $H^+(DMA)$ core
F	2922	2907	2902	2900	2900	2898	2898	2898	2898	2898	CH_2 antisymmetric stretch of the $[(CH_3)_2N]$ radical
G	2896	2890	2885	2882	2873	2870	2870	2868	2866	2866	CH_3 symmetric stretch of neutral DMA and the $[(CH_3)_2N]$ radical
H	2848	2847	2844	2841	2840	2840	2838	2838	2838	2838	Fermi resonance (the coupling between the C–H symmetric stretch and the C–H bending overtones) or minor contribution from other isomers
I	2804	2807	2801	2801	2801	2798	2795	2795	2795	2795	

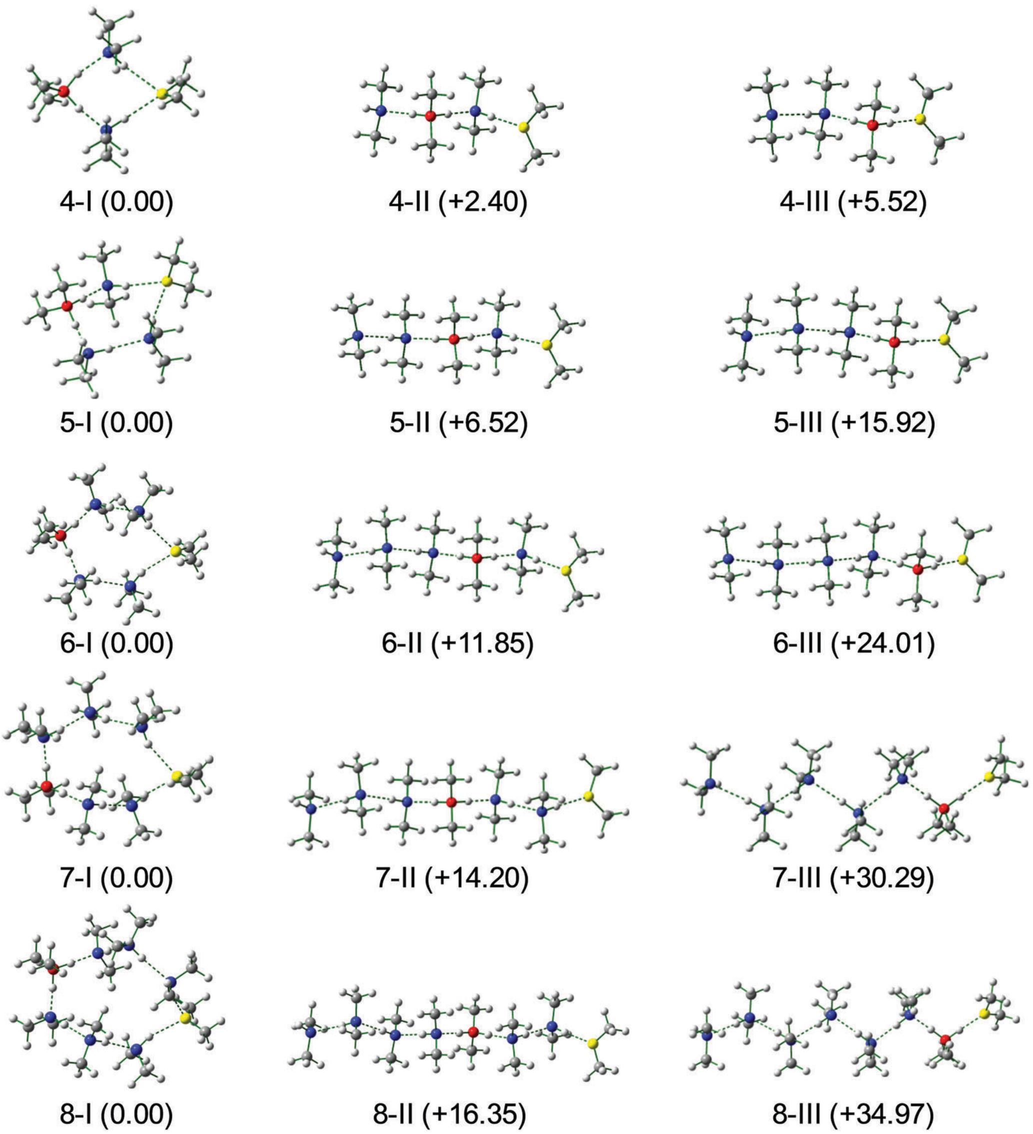

Fig. 3 Optimized structures of $(DMA)_n^+$ (n = 4–8) at the MPW1K/6-311+G(d,p) level of theory. The MP2/6-311+G(d,p)//MPW1K/6-311+G(d,p) calculated relative energies are given in kJ mol^{-1}. The N atom in the $(CH_3)_2NH_2^+$ ion core is highlighted as the red ball, the N atom in the $[(CH_3)_2N]$ radical is highlighted as the yellow ball, and the N atom in the neutral DMA molecule is highlighted as the blue ball, respectively.

experimental band F (2922 cm^{-1}). The calculated band g at 2890 cm^{-1} is due to the CH_3 symmetric stretch of neutral DMA and the $[(CH_3)_2N]$ radical, which is consistent with the experimental band G (2896 cm^{-1}). The calculated intense band at 2550 cm^{-1} is due to the H-bonded N–H stretch of the $(CH_3)_2NH_2^+$ ion core, which is not well resolved in the experimental spectra. In the simulated IR spectra of 4-II and 4-III, the positions of band b are close to the center of the experimental

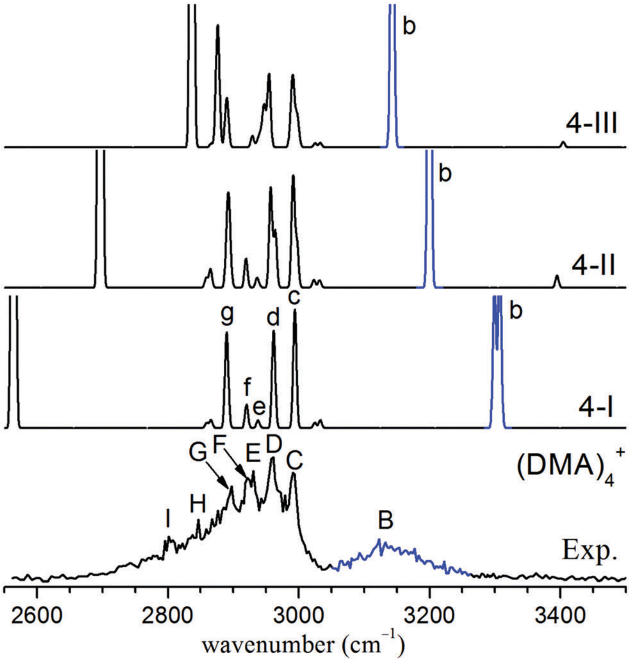

Fig. 4 Comparison of the experimental IRMPD spectrum of $(DMA)_4^+$ (bottom panel) with the MPW1K/6-311+G(d,p) calculated IR spectra of the three conformers (upper panels). The blue band is the marker of the H-bonded N–H stretch of 1-coord DMA (band b).

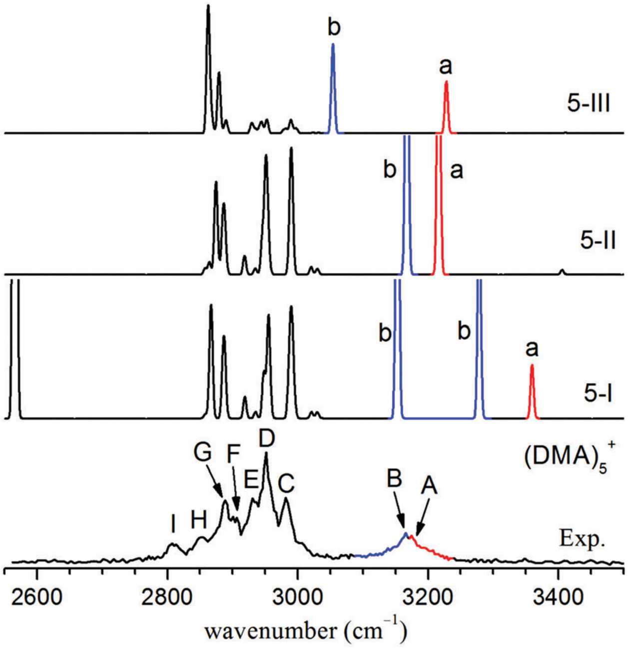

Fig. 5 Comparison of the experimental IRMPD spectrum of $(DMA)_5^+$ (bottom panel) with the MPW1K/6-311+G(d,p) calculated IR spectra of the three conformers (upper panels). The blue band is the marker of the H-bonded N–H stretch of 1-coord DMA (band b) and the red band is the marker of the H-bonded N–H stretch of 2-coord DMA (band a).

band B; the positions of bands c–g are almost the same as those of 4-I with slightly different intensities; the H-bonded N–H stretch modes (2696 cm^{-1} in 4-II and 2837 cm^{-1} in 4-III) of the $(CH_3)_2NH_2^+$ ion core are also not well resolved. Note that due to the hydrogen bond fluctuations, the integrated intensities of the sharp peak b in the harmonic spectra of 4-I, 4-II, and 4-III could be distributed over a much larger energy range. Such broadening of vibrational features in the H-bonded clusters has been interpreted by molecular dynamics simulations.[25–27]

To summarize, the calculated IR spectra of isomers 4-I, 4-II, and 4-III qualitatively reproduce the experimental IRMPD spectrum of $n = 4$, except that bands H and I are not reproduced theoretically. The tentative assignment for bands H and I is Fermi resonance or minor contribution from other isomers, wherein the positions are very similar to those in the $(TMA)_n^+$ clusters.[17] Recent *ab initio* anharmonic calculations of neutral monomethylamine $(MMA)_n$ (n = 2–4) clusters demonstrated that this Fermi resonance is stemmed from the coupling between the C–H symmetric stretch and C–H bending overtones.[28] In the $(DMA)_4^+$ cluster, the intensities of calculated bands c–g are somewhat different from the experimental bands C–G, which would also be attributed to the Fermi resonance as detailed for $(MMA)_n$ systems.[28] Due to the expensive computational cost, *ab initio* anharmonic calculations were not carried out for the $(DMA)_n^+$ clusters here.

$(DMA)_5^+$

The lowest energy isomer for $(DMA)_5^+$, 5-I, could be viewed as the derivative of 4-I, in which the fifth DMA molecule is inserted into the ring structure *via* a N···H intermolecular interaction, as shown in Fig. 3. Isomer 5-II consists of a chain structure with an ion-radical separated pair, which lies 6.52 kJ mol^{-1} higher than isomer 5-I. Isomer 5-III has a chain structure with an ion-radical contact pair, which lies 15.92 kJ mol^{-1} higher than 5-I. The simulated IR spectra of 5-I and 5-II nicely reproduce the experimental $n = 5$ spectrum in the C–H stretch region (2800–3000 cm^{-1}) (Fig. 5). The contribution for the experimental spectrum could be mainly from isomers 5-I and 5-II. The minor contribution of 5-III cannot be ruled out, because its spectrum matches to the part of the experimental spectrum.

$(DMA)_6^+$

The lowest-energy isomer (6-I) is a ring structure, in which the $[(CH_3)_2N]$ radical is separated from the $(CH_3)_2NH_2^+$ ion core by two DMA molecules (Fig. 3). Isomer 6-II could be viewed on the basis of 5-II, and the sixth DMA forms a hydrogen bond with the terminal neutral DMA molecule, which lies 11.85 kJ mol^{-1} higher than isomer 6-I. The structure with an ion-radical contact pair for $(DMA)_6^+$ (6-III) lies 24.01 kJ mol^{-1} above 6-I. The simulated IR spectrum of 6-I is in accord with experiment (Fig. 6), in which the calculated band positions of the H-bonded N–H stretch of 1-coord DMA (band b) are close to the center of the experimental band B, and the calculated band position of the H-bonded N-H stretch of 2-coord DMA (band a) is close to the upper edge of broad band A. The calculated IR spectrum of 6-II in the C–H stretch region is very similar to that of 6-I. In the simulated IR spectrum of 6-III, band b is calculated at

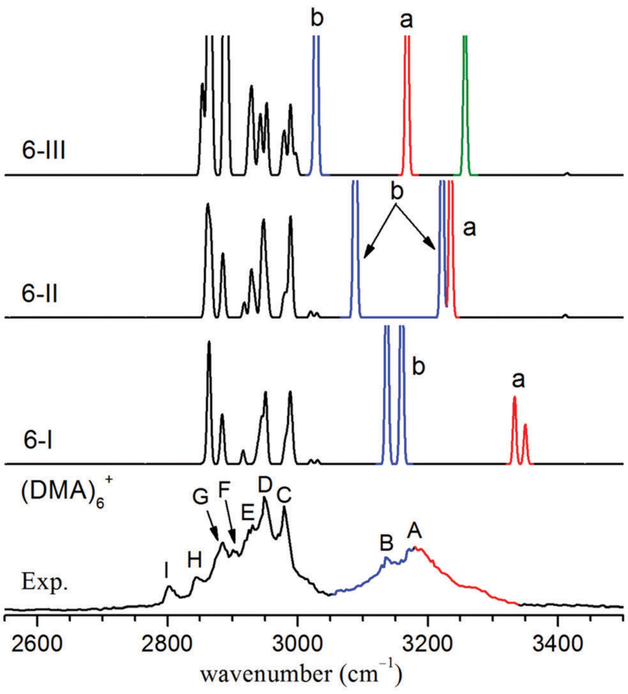

Fig. 6 Comparison of the experimental IRMPD spectrum of $(DMA)_6^+$ (bottom panel) with the MPW1K/6-311+G(d,p) calculated IR spectra of the three conformers (upper panels). The blue band is the marker of the H-bonded N–H stretch of 1-coord DMA (band b), the red band is the marker of the H-bonded N–H stretch of 2-coord DMA (band a), and the olive band is the marker of the H-bonded N–H stretch of 3-coord DMA.

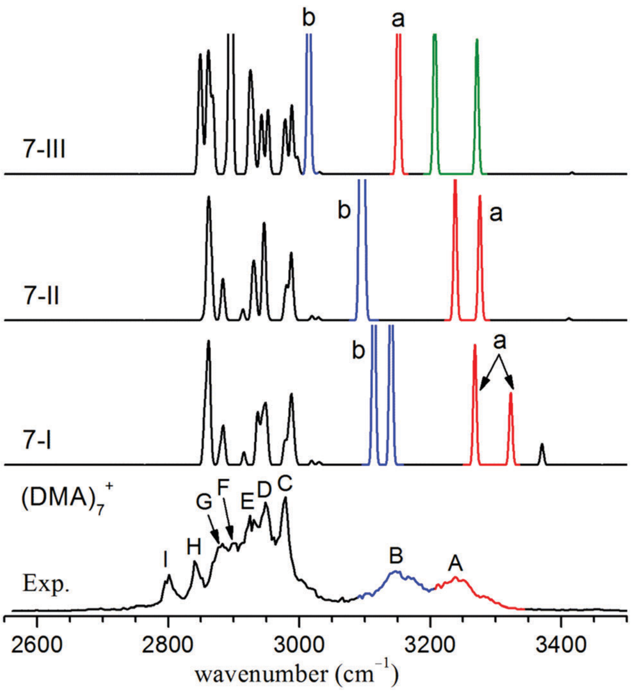

Fig. 7 Comparison of the experimental IRMPD spectrum of $(DMA)_7^+$ (bottom panel) with the MPW1K/6-311+G(d,p) calculated IR spectra of the three conformers (upper panels). The blue band is the marker of the H-bonded N–H stretch of 1-coord DMA (band b), the red band is the marker of the H-bonded N–H stretch of 2-coord DMA (band a), and the olive band is the marker of the H-bonded N–H stretch of 3-coord (or greater) DMA.

3000 cm^{-1} and an intense band of the H-bonded N–H stretch of 3-coord DMA is calculated at 3260 cm^{-1}, respectively. Isomers 6-I and 6-II could be dominated in $(DMA)_6^+$.

$(DMA)_n^+$ (*n* = 7 and 8)

The lowest-energy isomers of 7-I and 8-I have the ion-radical separated pair forming the ring structures (Fig. 3). Isomers 7-II and 8-II consist of the chain structures with the ion-radical separated pair. Isomers 7-III and 8-III are featured by the ion-radical contact pair. As shown in Fig. 7 and 8, the calculated IR spectra of isomers 7-I/8-I agree the best with the experimental spectra, while those of isomers 7-II/8-II and 7-III/8-III also match to the part of the experimental spectra, indicating that the major contribution would be from isomers 7-I/8-I and the minor contribution from isomers 7-II/8-II and 7-III/8-III.

5. Discussion

The overall agreement between the experimental and calculated infrared spectra has been obtained, which allows for extracting the general trends in the structural evolution of the $[(CH_3)_2NH]_n^+$ clusters. For *n* = 4, the $(CH_3)_2NH_2^+$–$[(CH_3)_2N]$ ion-radical separated pair and the ion-radical contact pair could coexist. The *n* = 5 and 6 clusters are dominated by the ion-radical separated pair with the ring and chain structures. The ion-radical separated pairs with the ring structures are mainly responsible for *n* = 7 and 8. It should be noted that the minor contributions of the ion-radical contact pair are not excluded, because their spectra are also in agreement with the part of the observed spectra. These results show that the $[(CH_3)_2NH]_n^+$ clusters should be regarded as the proton-transferred $H^+[(CH_3)_2NH]_{n\text{-}1}[(CH_3)_2N]$ motifs. Analogously, previous studies on the $(NH_3)_n^+$ (*n* = 2–4) clusters have indicated that the dimer cation has the proton-transferred NH_4^+–NH_2 structure, in which the motif is retained in the trimer and tetramer cations.[15] In contrast, the charge-shared N···N type $(TMA)_2^+$ ion core is preferred in the cold cationic trimethylamine $(TMA)_n^+$ clusters,[17] and the proton-transferred C···HN type structure appears in the warmer ion sources.[16] At the G4(MP2) level, the reaction energies for reactions (3), (4), and (5) are calculated to be exothermic by 71.55, 28.55, and 7.39 kJ mol^{-1}, respectively. This suggests that proton transfer is much more favorable for NH_3^+ and $(CH_3)_2NH^+$ than for $(CH_3)_3N^+$, supporting the aforementioned experimental observations.

$$NH_3^+ + NH_3 \rightarrow NH_4^+ + NH_2 \quad (3)$$

$$(CH_3)_2NH^+ + (CH_3)_2NH \rightarrow (CH_3)_2NH_2^+ + (CH_3)_2N \quad (4)$$

$$(CH_3)_3N^+ + (CH_3)_3N \rightarrow (CH_3)_3NH^+ + (CH_3)_2NCH_2 \quad (5)$$

The $(CH_3)_2NH_2^+$–$[(CH_3)_2N]$ ion-radical contact pair should be generated during the primary event in the ionization of dimethylamine. It can be inferred from the aforementioned analysis that in the cationic $(DMA)_n^+$ clusters, the $[(CH_3)_2N]$ radical is separated from the $(CH_3)_2NH_2^+$ ion core by one DMA molecule at *n* = 4–6 and by two or more DMA molecules

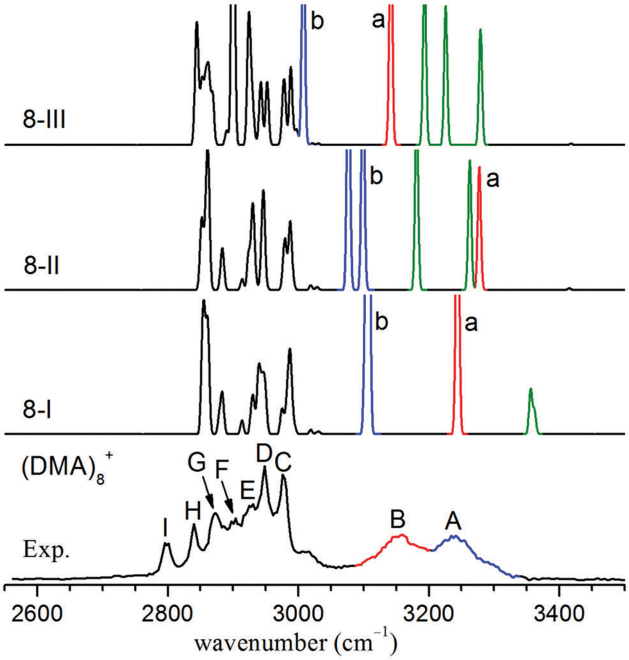

Fig. 8 Comparison of the experimental IRMPD spectrum of $(DMA)_8^+$ (bottom panel) with the MPW1K/6-311+G(d,p) calculated IR spectra of the three conformers (upper panels). The blue band is the marker of the H-bonded N–H stretch of 1-coord DMA (band b), the red band is the marker of the H-bonded N–H stretch of 2-coord DMA (band a), and the olive band is the marker of the H-bonded N–H stretch of 3-coord (or greater) DMA.

in the larger clusters. This implies that the $(CH_3)_2NH_2^+$–$[(CH_3)_2N]$ ion-radical contact pair is not stable in the subsequent radiation-induced processes of DMA, and the $[(CH_3)_2N]$ radical is released from the charged site in the cationic DMA networks. The reactivity of the $[(CH_3)_2N]$ radical could increase with increasing cluster size as compared to the contact pair. Previous studies showed that the nascent H_2O^+ water cation reacts with H_2O on a femtosecond scale to form H_3O^+–OH.[29,30] In alcohols, these timescales can extend to many picoseconds, because the alkyl tails limit ideal solvation structures and hinder the reorientation dynamics required to optimally interact with a solute.[31] Therefore, the present system provides an interesting model for further time-resolved studies aimed at unraveling the dynamics of proton transfer in dimethylamine networks, which would enrich the fundamental understanding of various ionizing radiation-induced processes relevant to chemical, biological, and atmospheric environments.

6. Conclusion

The infrared spectra of $(DMA)_n^+$ (n = 4–13) in the gas phase were recorded in the 2500–3500 cm^{-1} spectral range. The combination of experimental and calculated IR spectra allows for an identification of the general trends in the stepsize formation of ion-radical networks in the $(DMA)_n^+$ complexes. The nominal $(DMA)_n^+$ clusters should be regarded as the proton-transferred $H^+[(CH_3)_2NH]_{n-1}[(CH_3)_2N]$ motifs. The coexistence of the $(CH_3)_2NH_2^+$–$[(CH_3)_2N]$ ion-radical separated pair and the ion-radical contact pair is likely for n = 4. The $[(CH_3)_2N]$ radical is separated from the $(CH_3)_2NH_2^+$ ion core by at least one DMA molecule in the $n \geq 5$ clusters. The mobility of the $[(CH_3)_2N]$ radical could increase with increasing cluster size.

Conflicts of interest

The authors declare no competing financial interest.

Acknowledgements

This work was supported by the National Natural Science Foundation of China (Grants 21673231 and 21688102), the Strategic Priority Research Program of the Chinese Academy of Sciences (CAS) (Grant No. XDB17000000), the Dalian Institute of Chemical Physics (DICP DCLS201702), and the Dalian National Laboratory for Clean Energy (DNL), CAS.

References

1 B. C. Garrett, D. A. Dixon, D. M. Camaioni, D. M. Chipman, M. A. Johnson, C. D. Jonah, G. A. Kimmel, J. H. Miller, T. N. Rescigno, P. J. Rossky, S. S. Xantheas, S. D. Colson, A. H. Laufer, D. Ray, P. F. Barbara, D. M. Bartels, K. H. Becker, H. Bowen, S. E. Bradforth, I. Carmichael, J. V. Coe, L. R. Corrales, J. P. Cowin, M. Dupuis, K. B. Eisenthal, J. A. Franz, M. S. Gutowski, K. D. Jordan, B. D. Kay, J. A. LaVerne, S. V. Lymar, T. E. Madey, C. W. McCurdy, D. Meisel, S. Mukamel, A. R. Nilsson, T. M. Orlando, N. G. Petrik, S. M. Pimblott, J. R. Rustad, G. K. Schenter, S. J. Singer, A. Tokmakoff, L. S. Wang, C. Wittig and T. S. Zwier, *Chem. Rev.*, 2005, **105**, 355–389.
2 A. Mozumder and J. L. Magee, *J. Chem. Phys.*, 1966, **45**, 3332–3341.
3 X.-B. Wang, *J. Phys. Chem. A*, 2017, **121**, 1389–1401.
4 O. Dopfer and M. Fujii, *Chem. Rev.*, 2016, **116**, 5432–5463.
5 N. Heine and K. R. Asmis, *Int. Rev. Phys. Chem.*, 2015, **34**, 1–34.
6 A. B. Wolk, C. M. Leavitt, E. Garand and M. A. Johnson, *Acc. Chem. Res.*, 2014, **47**, 202–210.
7 A. Fujii and K. Mizuse, *Int. Rev. Phys. Chem.*, 2013, **32**, 266–307.
8 F. N. Keutsch, J. D. Cruzan and R. J. Saykally, *Chem. Rev.*, 2003, **103**, 2533–2577.
9 T. S. Zwier, *Annu. Rev. Phys. Chem.*, 1996, **47**, 205–241.
10 G. H. Gardeinier, M. A. Johnson and A. B. McCoy, *J. Phys. Chem. A*, 2009, **113**, 4772–4779.
11 K. Mizuse, J.-L. Kuo and A. Fujii, *Chem. Sci.*, 2011, **2**, 868–876.
12 K. Mizuse and A. Fujii, *J. Phys. Chem. A*, 2013, **117**, 929–938.
13 J. D. Herr, J. Talbot and R. P. Steele, *J. Phys. Chem. A*, 2015, **119**, 752–766.
14 J. D. Herr and R. P. Steele, *J. Phys. Chem. A*, 2016, **120**, 7225–7239.
15 M. Hachiya, Y. Matsuda, K.-i. Suhara, N. Mikami and A. Fujii, *J. Chem. Phys.*, 2008, **129**, 094306.

16 Y. Matsuda, Y. Nakayama, N. Mikami and A. Fujii, *Phys. Chem. Chem. Phys.*, 2014, **16**, 9619–9624.

17 X. Lei, X. Kong, Z. Zhao, B. Zhang, D. Dai, X. Yang and L. Jiang, *Phys. Chem. Chem. Phys.*, 2018, **20**, 25583–25591.

18 R. Zhang, A. Khalizov, L. Wang, M. Hu and W. Xu, *Chem. Rev.*, 2012, **112**, 1957–2011.

19 B. Noziere, M. Kaberer, M. Claeys, J. Allan, B. D'Anna, S. Decesari, E. Finessi, M. Glasius, I. Grgic, J. F. Hamilton, T. Hoffmann, Y. Iinuma, M. Jaoui, A. Kahno, C. J. Kampf, I. Kourtchev, W. Maenhaut, N. Marsden, S. Saarikoski, J. Schnelle-Kreis, J. D. Surratt, S. Szidat, R. Szmigielski and A. Wisthaler, *Chem. Rev.*, 2015, **115**, 3919–3983.

20 K. Luria, N. Lavie and U. Even, *Rev. Sci. Instrum.*, 2009, **80**, 104102.

21 W. R. Bosenberg and D. R. Guyer, *J. Opt. Soc. Am. B*, 1993, **10**, 1716–1722.

22 M. J. Frisch, G. W. Trucks, H. B. Schlegel, G. E. Scuseria, M. A. Robb, J. R. Cheeseman, G. Scalmani, V. Barone, B. Mennucci, G. A. Petersson, H. Nakatsuji, M. Caricato, X. Li, H. P. Hratchian, A. F. Izmaylov, J. Bloino, G. Zheng, J. L. Sonnenberg, M. Hada, M. Ehara, K. Toyota, R. Fukuda, J. Hasegawa, M. Ishida, T. Nakajima, Y. Honda, O. Kitao, H. Nakai, T. Vreven, J. A. Montgomery Jr., J. E. Peralta, F. Ogliaro, M. J. Bearpark, J. Heyd, E. N. Brothers, K. N. Kudin, V. N. Staroverov, R. Kobayashi, J. Normand, K. Raghavachari, A. P. Rendell, J. C. Burant, S. S. Iyengar, J. Tomasi, M. Cossi, N. Rega, N. J. Millam, M. Klene, J. E. Knox, J. B. Cross, V. Bakken, C. Adamo, J. Jaramillo, R. Gomperts, R. E. Stratmann, O. Yazyev, A. J. Austin, R. Cammi, C. Pomelli, J. W. Ochterski, R. L. Martin, K. Morokuma, V. G. Zakrzewski, G. A. Voth, P. Salvador, J. J. Dannenberg, S. Dapprich, A. D. Daniels, O. Farkas, J. B. Foresman, J. V. Ortiz, J. Cioslowski and D. J. Fox, *Gaussian 09*, Gaussian, Inc., Wallingford, CT, USA, 2009.

23 J. P. Merrick, D. Moran and L. Radom, *J. Phys. Chem. A*, 2007, **111**, 11683–11700.

24 L. A. Curtiss, P. C. Redfern and K. Raghavachari, *J. Chem. Phys.*, 2007, **127**, 124105.

25 L. Jiang, S.-T. Sun, N. Heine, J.-W. Liu, T. I. Yacovitch, T. Wende, Z.-F. Liu, D. M. Neumark and K. R. Asmis, *Phys. Chem. Chem. Phys.*, 2014, **16**, 1314–1318.

26 S.-T. Sun, L. Jiang, J. W. Liu, N. Heine, T. I. Yacovitch, T. Wende, K. R. Asmis, D. M. Neumark and Z.-F. Liu, *Phys. Chem. Chem. Phys.*, 2015, **17**, 25714–25724.

27 X. Kong, S.-T. Sun, L. Jiang and Z.-F. Liu, *Phys. Chem. Chem. Phys.*, 2018, **20**, 4571–4578.

28 Q.-R. Huang, Y.-C. Li, K.-L. Ho and J.-L. Kuo, *Phys. Chem. Chem. Phys.*, 2018, **20**, 7653–7660.

29 C. Y. Yang, K. F. Wong, M. S. Skaf and P. J. Rossky, *J. Chem. Phys.*, 2001, **114**, 3598–3611.

30 R. Jimenez, G. R. Fleming, P. V. Kumar and M. Maroncelli, *Nature*, 1994, **369**, 471–473.

31 S. J. Rosenthal, R. Jimenez, G. R. Fleming, P. V. Kumar and M. Maroncelli, *J. Mol. Liq.*, 1994, **60**, 25–56.